Application of Transmural Flow Across In Vitro Microvasculature Enables Direct Sampling of Interstitial Therapeutic Molecule Distribution

Citation: Offeddu, Giovanni et al. "Application of Transmural Flow Across In Vitro Microvasculature Enables Direct Sampling of Interstitial Therapeutic Molecule Distribution." Small 15, 46 (November 2019): 1902393 © 2019 Wiley

As Published: http://dx.doi.org/10.1002/SMLL.201902393

Publisher: Wiley

Persistent URL: https://hdl.handle.net/1721.1/128270

Version: Author's final manuscript: final author's manuscript post peer review, without publisher's formatting or copy editing

Application of transmural flow across *in vitro* microvasculature enables direct sampling of interstitial therapeutic molecule distribution

Giovanni S. Offeddu, Luca Possenti, Joshua T. Loessberg-Zahl, Paolo Zunino, John Roberts, Sean Han, Dean Hickman, Charles G. Knutson, Roger D. Kamm**

Dr. G. S. Offeddu, Prof. R. D. Kamm
Department of Biological Engineering, Massachusetts Institute of Technology, Cambridge MA, USA
E-mail: rdkamm@mit.edu

Dr. L. Possenti
LaBS, Department of Chemistry, Materials and Chemical Engineering, Politecnico di Milano, Milan, Italy

Mr. J. T. Loessberg-Zahl
BIOS Lab-on-a-Chip Group, University of Twente, Enschede, The Netherlands

Prof. P. Zunino
MOX, Department of Mathematics, Politecnico di Milano, Milan, Italy

Mr. J. Roberts, Dr. X. Han, Dr. D. Hickman, Dr. C. G. Knutson
Amgen Discovery Research, Amgen Inc., 360 Binney Street, Cambridge MA, USA
E-mail: charlie.knutson@amgen.com

Keywords: trans-endothelial transport, organ-on-chip, biotherapeutics and biologics, permeability, hydraulic conductivity

In vitro prediction of physiologically-relevant transport of therapeutic molecules across the microcirculation represents an intriguing opportunity to predict efficacy in human populations. On-chip microvascular networks (MVNs) show physiologically-relevant values of molecular permeability, yet like most systems, they lack an important contribution to transport: the ever-present fluid convection through the endothelium. Quantification of transport through the MVNs by current methods also requires confocal imaging and advanced analytical techniques, which can be a bottleneck in industry and academic laboratories. Here, it is shown that by recapitulating physiological transmural flow across the MVNs, the concentration of small and large molecule therapeutics can be directly sampled in the interstitial fluid and analyzed using standard analytical techniques. The magnitudes of transport measured in MVNs reveal trends with molecular size and type (protein *vs*. non-protein) that are expected *in vivo*, supporting the use of the MVNs platform as an *in vitro* tool to predict distribution of therapeutics *in vivo*.

1. Introduction

Organ-on-chip technologies are attracting increased attention because of their potential to better recapitulate and explore complex human biological interactions compared to conventional *in vitro* systems [1, 2]. A promising application is that of drug discovery and development, where limitations arise with the use of animal models in reproducing critical aspects of human biology [3]. Organ-on-chip technologies can reduce our reliance on animal testing and inform safety assessments by testing novel molecules directly in physiologically-relevant, human-derived tissues. Systems that allow the measurement of fundamental aspects of drug safety, pharmacokinetics and efficacy, therefore, hold great potential value for patients. In particular, three-dimensional (3D) models of the human microvasculature (endothelium-on-chip, made by bioprinting [4], casting [5], or combination approaches [6], among others) can be used to quantify the distribution of circulating therapeutic molecules across the capillary wall into the interstitial space where they access cellular targets and elicit pharmacological response [7].

In vivo, therapeutic molecules can cross the endothelium in several ways, the specific contributions of which are primarily determined by the physicochemical properties of the particular therapeutic, such as size, charge, and ability to bind endothelial membrane transport proteins [8]. Many small molecule therapeutics can passively diffuse across the endothelial cell membrane [9], while large molecule therapeutics may only passively distribute across the endothelium if their size permits passage through endothelial cell junctions (< 10 nm in diameter [10]), in which case the molecules are carried through the endothelium by transmural fluid flow [11]. Larger molecules and nanoparticles (up to 80-100 nm [12, 13]), instead, likely require active cellular transport (transcytosis) through endothelial cell vesicles. In order to successfully predict therapeutic molecule distribution *in vivo*, an *in vitro* system must be capable of recapitulating not only the magnitude of transport, but also the particular paths through which therapeutics cross the endothelium.

Self-assembled microvascular networks (MVNs) made of primary endothelial and stromal cells can be formed as part of microfluidic devices, where they take on a fully perfusable 3D capillary bed morphology enclosed within a hydrogel matrix [14, 15]. These MVNs have been shown to possess values of endothelial permeability that are comparable to those measured in animals and humans for a variety of molecules [16]. As observed *in vivo*, tight endothelial junctions in the MVNs limit the paracellular passage of large proteins, which are instead actively shuttled across the cells through vesicular transport. This quality makes the MVNs clearly outperform other *in vitro* systems, such as endothelial monolayers in transwells, where permeability values can be up to three orders of magnitude higher [16, 17]. However, compared to transwell systems where fluid across the monolayer can be directly sampled, MVNs are typically formed in a closed system, which hinders direct fluid sampling and requires imaging-based measurements. In order to make physiologically-relevant measurements of therapeutics distribution across the MVNs, fluorescently-labeled molecules are required, which may have altered biodistribution due to increased size (relevant for small molecule therapeutics) or to different binding to transporters (relevant for large molecule therapeutics). Additionally, a need exists for higher-throughput measurements, which are compromised by imaging-based assessments that require advanced analysis to capture and quantify molecular extravasation.

In this work, the important contribution of transmural flow to the extent of molecular flux to the tissue compartment was recapitulated for the first time in the MVNs using physiological levels of pressure across the endothelium. Further, because transmural fluid continues flowing through the interstitial matrix and eventually exits the MVNs device, it can be collected and analyzed by standard analytical techniques like ELISA, which do not rely on a fluorescent tag. Model molecules of varying physicochemical and biological properties, including both small and large therapeutic molecules, were perfused through the system, recapitulating important trends that reflect *in vivo* biodistribution. The results reported here

further demonstrate the physiological relevance of the MVNs for the *in vitro* measurement of drug transport in the human microcirculation.

2. Results and Discussion

2.1. Perfusion and hydraulic conductivity of MVNs

The recapitulation of physiological transmural flow requires the creation of a pressure differential across the endothelium. The MVNs form within the central gel channel of a three-channel microfluidic device, where they bridge the side channels containing cell culture medium **(Figure 1a)**. An additional endothelial monolayer is formed on the gel channel sides, which integrates with the MVNs and limits direct diffusion from the cell culture medium into the hydrogel matrix [16]. All three device channels possess two inlets, used in the case of the gel channel to inject the cell mixture during fabrication, and in the case of the side channels to change cell culture medium daily. By using a pressure regulator connected to the open inlets of both side channels (Figure 1b), this medium can be pressurized, thereby inducing a pressure differential between the side channels and the open gel ports. The presence of continuous fluid within the perfused MVNs (Figure 1c) ensures that the entire endothelium is subjected to the differential pressure, producing transmural flow into the hydrogel matrix.

In the body, the total pressure differential in the microcirculation is due to two contributions: hydrostatic and oncotic pressures. Hydrostatic pressure originates from pumping of the heart, and within the microcirculation has a magnitude of approximately 4 - 5 kPa [18], resulting in flow *out of* the circulation (apical to basal). Conversely, oncotic pressure derives from the higher concentration of plasma proteins, mostly albumin and immunoglobulin G (IgG) [19], within the blood compared to the tissue compartment, resulting in flow *into* the circulation (basal to apical). Oncotic flow is driven by a pressure of approximately 3 - 4 kPa [18], resulting in a net pressure differential across the microcirculation of approximately 1 - 2 kPa. This positive transmural pressure gives rise to interstitial fluid flow, which enters into the lymphatic vascular network that returns it to the low-pressure venous circulation. Fluid flux per surface area of the endothelium, Q/SA, is given by the Starling equation [20]:

$$Q/SA = L_p\,(\Delta p - \sigma\Delta\pi) \quad (1)$$

where Δp and $\Delta\pi$ are the hydrostatic and oncotic pressure differentials, σ is the reflection coefficient (*i.e.* the fraction of plasma proteins in the blood that is not carried by the transmural flow), and L_p is the hydraulic conductivity of the endothelium. Together, L_p and σ contribute to the correct barrier function of the endothelium and its capacity to maintain homeostasis [11].

Within the MVNs, the net differential pressure was recapitulated entirely through hydrostatic pressure, as no oncotic pressure difference is present at steady state within the microfluidic device (medium serum concentration within and outside the lumens is equivalent). In order to investigate the effect of this physiological pressure differential on the MVN endothelium, a small (≈ 390 Da) tracer, fluorescein isothiocyanate (FITC), was perfused and its flux across the endothelium measured as a function of applied hydrostatic pressure **(Figure 2a)**. As transmural pressure, hence flow, increased, more solute was transported by convection through the endothelial junctions, which was measured as an increase in the apparent permeability to the solute, P_{app}, according to [11]:

$$P_{app} = P + L_p\,(1-\sigma)\,(\Delta p - \sigma\Delta\pi) \quad (2)$$

where P is the vessel permeability with no driving pressure, as is normally measured. Assuming no reflection of FITC by the endothelium due to its small size (σ = 0), the linear increase (*p-value* < 0.05, R^2 = 0.98) in P_{app} can be fit by Equation 2 to yield L_p for the MVNs as 4.37 x 10^{-12} m s^{-1} Pa^{-1}.

Figure 2b shows a comparison of this hydraulic conductivity with those of *in vitro* endothelial monolayers [21-29], as well as data from animal models and humans [18, 30]. The MVNs show one to two orders of magnitude lower L_p compared to the majority of other *in vitro* models (10^{-12} compared to 10^{-10}-10^{-11}), and, instead, a value comparable to *in vivo* animal models (10^{-12} for the non-specialized microvasculature of the rabbit, dog and cat). Notably, for both *in vitro* and *in vivo* models the lowest L_p values are those for brain endothelial cells (*in vitro*, only mouse brain endothelial cells produced a lower value than what was measured for

the MVNs), likely due to the increased tightness of the junctions making up the blood-brain barrier [31]. Conversely, the only *in vivo* value significantly larger than what was measured for the MVNs was that of the frog mesentery, where the need for nutrient intake likely mandates greater amounts of fluid transport [32]. The physiological value of hydraulic conductivity of the MVNs ultimately depends on the small dimension of the endothelial junctions, as well as on the presence of a functional glycocalyx in this system [16], imposing a larger barrier to fluid transport [20]. These factors contribute to the observed physiological values of permeability in the MVNs, further supporting the importance of more complex *in vitro* endothelial models to predict distribution of therapeutics in the body.

2.2. Effect of transmural flow on plasma protein transport

The ability to differentiate between passive and active transport pathways across the endothelium is of significant importance to establish a successful model of the microcirculation. Indeed, pathological states may affect passive and active passage differently [33], and so recapitulation of the magnitude of transport alone is not enough. Having established the baseline of hydraulic conductivity of the MVNs using a small molecule, a similar investigation of permeability as a function of pressure can provide insight into the capacity of large molecules to cross the endothelium. Dextrans are large molecule solutes that are not specifically recognized for transport by endothelial cells, so that their permeability proceeds primarily through endothelial junctions [16]. Figure 2c shows the increase in P_{app} with pressure for dextrans of increasing molecular weight (4, 40, 70 and150 kDa, R^2 = 0.96, 0.89, 0.94, 0.99, respectively, and *p-value* < 0.05 in all cases). The increase in P_{app} was found to be faster for smaller solutes, and the linear trends were fit to Equation 2 to yield the reflection coefficient (Figure 2d). It can be seen that σ increases (*p-value* < 0.05) with dextran molecular weight from 0.35 for 4 kDa to 0.78 for 150 kDa, indicating that less of the large molecules are carried by the transmural flow into the hydrogel matrix, which is consistent with the decreasing permeability of these molecules [16].

Plasma proteins like human serum albumin and IgG are primarily involved in maintaining homeostasis across the endothelium through the oncotic contribution to transmural flow. To maintain the correct osmotic pressure *in vivo*, their passage through the endothelium must be limited [19]. In the MVNs, contrary to what was observed for dextrans, the P_{app} of these proteins was not observed to increase with pressure (**Figure 3a**, *p-value* > 0.05). Any small increase in protein flux with pressure, if present, was hidden by the inherent variability of the measurements, indicating that $\sigma \approx 1$ for these molecules. This result is consistent with values of σ reported previously for albumin (0.83) and IgG (0.96) in animals [34]. Further, it is consistent with a mechanism of active transport for these molecules across the endothelium (*i.e.* transcytosis through active cellular recognition and vesicular transport, as previously reported [16, 35, 36]), which is unaffected by fluid convection through the endothelial junctions (Figure 3b).

Pressurization of the MVNs may produce changes in the endothelial junctions, potentially impacting passive solute flux. However, repeated cycles of pressurization were not found to alter the P_{app} measurements (Figure 3c) or the morphology of the endothelial junctions, as imaged by immunofluorescent staining of a tight junction marker, ZO1 (Figure 3d). Instead, the MVNs showed the ability to maintain structural integrity under physiological levels of pressure, as indicated by their consistent recovery during cycles of pressurization **(Video S1)**. Importantly, the results reported so far show that the MVNs can be used in conjunction with confocal microscopy and fluorescently-labelled molecules to make robust local measurements of concentration distribution across the endothelium in the presence of physiologically-relevant transmural pressure and flow.

2.3. Measurement and simulation of interstitial flow

Transmural flow from capillaries continues within the tissue compartment as interstitial flow, until it is collected by lymphatic vessels and eventually flows back into the circulation [37]. In

the system presented here, one of the gel ports was closed in order to direct all flow to the other (the "lymphatic") outlet. Interstitial flow is then the result of transmural flow from the MVNs, as well as from the endothelial monolayer lining the side of the gel channel, which is more permissive than the self-assembled microvessels likely due to the 2D morphology [16]. The overall fluid velocity magnitude was measured by fluorescent tracking of photobleached spots (**Video S2 and S3**) as a function of location within the device. The resulting velocity map is shown in **Figure 4a** in the case of an applied pressure of 1000 Pa. A pressure of 1000 Pa was used in all subsequent studies because it falls within the physiological range of the microcirculation.

The measured velocities were compared to computational simulations of interstitial fluid flow (Figure 4b and **Figure S1a**) for a range of hydraulic conductivities of the endothelial monolayer, varying between 1-fold (1X) and 500-fold (500X) of the hydraulic conductivity of the MVNs. Figure 4c shows the average interstitial fluid velocity as a function of distance from the outlet, which was observed to increase towards the outlet (*p-value* < 0.05). Comparison between the experimental data and simulated fluid velocities shows that the endothelial monolayer is approximately 100X more permissive to fluid than the MVNs, consistent with previously published monolayer results (Figure 2b). Notably, the resulting interstitial flow has an average velocity comparable to that reported *in vivo* (≈ 1.3 μm s^{-1} compared to 0.1 - 4 μm s^{-1} [11]).

For a given applied pressure, the hydraulic conductivity of the MVNs and side-monolayer determine the fluid pressure within the hydrogel matrix. If either conductivity is high enough, pressurization of the hydrogel would reduce the effective pressure differential across the endothelium. Computational simulation of the pressure within the hydrogel for the same range of monolayer L_p showed that in the present case (100X of MVNs, Figure 4d and Figure S1b) interstitial pressure ranged between approximately 2 and 15 Pa, values that are essentially negligible compared to the physiologically-relevant applied pressure (1000 Pa).

The presence of the endothelial monolayer alters the flow profile within the device. Indeed, transmural flow across the MVNs only, which in the system is supplied by a small amount (1 - 4 μm s^{-1}) of luminal flow from the side channels (Figure S2c and S2d), would result in much smaller interstitial fluid velocities, of the order of 0.1 μm s^{-1} (Figure 4c). This enhanced flow through the monolayer can be used advantageously to directly sample molecular concentrations in fluid crossing the endothelium, thereby providing a means to quantifying transport of non-fluorescent molecules, such as therapeutic agents, as described next.

2.4. Direct sampling of interstitial fluid

Interstitial fluid originating from the MVNs and the endothelial monolayer accumulates outside of the open gel outlet as a result of interstitial flow. As expected, the volume of extruded fluid within a set time increased with applied pressure (**Figure S2**), having an average flow rate of 1.2 μL s^{-1} when an intravascular pressure of 1000 Pa was applied. This extruded fluid can be collected to measure the concentration of any analyte perfused through the media channels. However, the precise measurement of molecular distribution across the MVNs requires separation from the signal coming from the monolayer, which is likely to be much larger due to a more permissive barrier.

The shape of the microfluidic device used here facilitates this separation, due to a difference in proximity of the MVNs and monolayer to the outlet. Indeed, the MVNs were observed to include perfusable vessels up to the outlet of the device, more than 3 mm away from the monolayer (**Figure 5a**). As a result, upon pressurization to 1000 Pa, the fluid collected was found to initially increase slightly in concentration and then remain approximately constant for 10 minutes (Figure 5b), after which the concentration rose to values comparable to what was perfused within the side channels of the device. This behavior can be interpreted by considering that when fluid flow is initiated, there will be a delay before the solute front flowing from the distant endothelial monolayer reaches the outlet and dominates the measurement.

During this time, the fluid flowing ahead of the front is largely displaced by fluid extruded purely from the MVNs in the proximity of the outlet.

In order to analyze solute transport across the MVN endothelium one can express the concentration of solute in the extruded fluid (the MVN equivalent of interstitial fluid *in vivo*), c, as a fraction of that of the perfused fluid (the MVN equivalent of blood/plasma), c_0. This normalized concentration ratio is often similarly used in animal model tests of drug biodistribution [38], as c and c_0 are parameters that can be easily measured without real-time imaging in the live specimens. The ratio can be expressed in terms of endothelial transport parameters, by considering that c will be the ratio between solute (J_s) and fluid (Q) fluxes across the endothelium:

$$c = J_s/Q \tag{3}$$

For large molecule therapeutics (> 1 kDa), solute flux will be the sum of diffusion through cell junctions and active transcellular transport, quantified by the permeability of the endothelium through a surface area SA, and convection of the solute across the junctions, a function of Q (from Equation 1), so that:

$$J_s = P\,SA\,(c_0 - c) + Q(1-\sigma)c_0 \tag{4}$$

Rearrangement of Equation 3 yields:

$$\frac{c}{c_0} = \frac{P+L_p\Delta p(1-\sigma)}{P+L_p\Delta p} \tag{5}$$

Where Δp represents the pressure difference across the endothelium.

In the analysis above, it is assumed that solute is uniformly distributed in the hydrogel matrix encompassing the MVNs, and that the loss of solute as it flows through this matrix, either due to filtration or chemical binding, is negligible. The former assumption is supported by the fact that the MVNs maintain a perfusable, uniform 3D morphology up to the outlet (**Figure S3**). The latter assumption is supported both by the high porosity and inter-fiber spacing of the matrix (**Figure S4a**), much larger than the nanometer-sized protein perfused (i.e.

albumin and IgG), and that c/c_0 is approximately unity for all solutes after the monolayer solute front reaches the gel outlet, supporting the assumption that binding is negligible to the gel matrix. In addition, measurements of interstitial fluid velocity as a result of a pressure difference between the two side channels and across a cell-free gel region (Figure S4b) revealed a hydraulic permeability of the matrix equal to 4.88 x 10^{-10} m^2 s^{-1} Pa^{-1}, comparable to highly permissive sponge materials used for the engineering of large tissues [39]. Consistently, measurements of the diffusion coefficient in the matrix, D_S, for dextran of varying molecular weight, albumin and IgG (Figure S4c and S4d), yielded values within 60% to 100% of their respective diffusion coefficients in fluid, D_0, setting a high baseline of diffusive transport to be further enhanced by convection.

Figure 5c shows values of c/c_0 for dextran, obtained through fluorescence analysis of the extruded fluid in a plate reader, where the ratio was observed to decrease with increasing molecular weight. Importantly, the model based on the endothelial transport parameters for these large molecules was found to successfully predict the experimental values measured in the system. A similar successful prediction was also obtained for albumin and IgG (Figure 5d), using reported values for σ [34], whereby the c/c_0 ratio for the two proteins was measured not only by fluorescence, but also through ELISA. Here, c/c_0 for albumin was found to be larger than for IgG, consistent with the permeability measurements for these proteins [16].

Finally, these MVNs were used to test the transport of clinically relevant therapeutic molecules. Figure 5e reports data for c/c_0 of two large protein-based therapeutics, Trastuzumab and Cetuximab, which are monoclonal antibodies used in the treatment of breast cancer to target the HER2 and EGF receptors, respectively [40, 41], and two common small chemotherapeutic drugs, Paclitaxel and Doxorubicin. Trastuzumab and Cetuximab produced values of c/c_0 comparable to those of human serum IgG (IgG: 0.10 ± 0.07, Trastuzumab: 0.06 ± 0.04, Cetuximab: 0.04 ± 0.02, *p-value* > 0.05 for all pairs). Such ratios, obtained for therapeutically-relevant un-tagged molecules, are comparable to those measured for monoclonal antibodies in

a variety of animal and human organs, including the lung, heart, muscles, and skin (0.04 – 0.15 [38]), and are particularly applicable given the clinically-relevant perfused concentration used (20 μg mL^{-1}, compared to a typical 10 – 65 μg mL^{-1} antibody concentration in patients' serum [42]). The values measured for Paclitaxel and Doxorubicin, with molecular weights of 854 and 544 Da, respectively, were initially found to be comparable to, or smaller than, those of the larger dextrans previously perfused (0.18 and 0.42, respectively, compared to the 0.25 - 0.77 range for dextrans), implying c/c_0 values of much larger molecules. However, these values were corrected by accounting for binding of the small molecules to serum present in the cell culture medium, a normal phenomenon *in vivo* [43]. These results, appropriately corrected for protein binding, showed a c/c_0 ratio close to unity for the two molecules, as expected from their small size, and, interestingly, higher for Paclitaxel than Doxorubicin (*p-value* < 0.05) despite the larger size of Paclitaxel. These results highlight the use of MVNs as a platform amenable to testing physiologically-relevant endothelial transport of small and large molecule therapeutics in the presence of transmural flow, revealing important trends in distribution across the endothelium depending on the particular molecule.

3. Conclusion

The MVN microfluidic platform is a tool that possesses the capability to predict both the magnitude and mode of transport of therapeutic molecules across the human microvascular endothelium. Through the induction of physiological rates of transmural and interstitial flow, the platform also gains an engineering benefit in that molecular concentrations can now be sampled directly in fluid flowing from the device, the MVN equivalent of interstitial fluid. This allows the use of standard analytical techniques used in academic and industry laboratories, without sacrificing the high-resolution imaging capabilities already offered by the platform. As such, the MVNs represent a versatile and robust system to test drug distribution with greater potential translation to outcomes in human populations.

4. Experimental Section

Fabrication of MVNs devices: MVNs form by self-assembly of endothelial and stromal cells, and the general method used to seed MVNs within microfluidic devices is detailed in [44]. Here, the MVNs were formed within three-channel microfluidic devices with large width channels (gel channel width of 3 mm, height of 500 μm [16]) to allow quantitative measurements of transport across the MVNs without interference from diffusion from the media channels. The device makes use of a guide-edge to hold the gel mixture within the central channel upon injection. Pooled Human Umbilical Vein Endothelial Cells (HUVECs, Angio-Proteomie, US), HUVECs GFP (Angio-Proteomie, US), and normal Human Lung Fibroblasts (nHLFs, Lonza, US) were cultured in collagen-coated flasks (Corning, US) in a controlled 5 % CO_2 atmosphere at 37 °C (used throughout for cell culture), with Vasculife Endothelial Medium (Lifeline LL-0003) and Fibrolife Fibroblast Medium (Lifeline LL-0011), respectively, and frozen following three passages. Upon thaw and sub-culture in un-coated flasks, the cells were seeded in fibrin gel as described in [44], at a final concentration of 6 million endothelial cells mL^{-1} and 2 million fibroblasts mL^{-1}. The cell mixture within the device was cultured over 7 days with daily Vasculife medium replacement. Excess HUVECs after seeding were re-plated and used at day 4 to form a monolayer on the side of the gel channel. For this, the endothelial cells were resuspended at 1 million cells mL^{-1}, and 40 μL of cell suspension was added to each media channel sequentially with a hold time of 10 minutes each, during which time the device was held vertically so that gravity would deposit cells evenly on the side of the gel channel. The MVNs became perfusable between day 5 and 6, and were used throughout the studies at day 7.

Antibodies and reagents: The MVNs were perfused with fluorescein-conjugated dextran (4, 40, 70, and 150 kDa, 0.1 mg mL^{-1} in Vasculife, supplied by Sigma Aldrich, US), human serum albumin (0.1 mg mL^{-1}, ab8030, Abcam, US), and human immunoglobulin G (0.1 mg mL^{-1}, IgG,

F9636, Sigma Aldrich, US), as well as Trastuzumab (20 μg mL^{-1}, MAB9589, R&D Systems, US), Cetuximab (20 μg mL^{-1}, MAB9577, R&D Systems, US), Oregon Green-conjugated Paclitaxel (2 μM, P22310, Thermofisher, US), and Doxorubicin (2 μM, D1515, Sigma Aldrich, US). Immunostaining of the MVNs was performed using a monoclonal ZO1 antibody (33-91100, Invitrogen, US).

Solute and fluid perfusion, and permeability assessment: Solute-containing medium was perfused through the MVNs by the introduction of ~50 Pa pressure drop between the two medium channels. Two FlowEz pressure regulators (Fluigent, US) were connected by tubing to an open port of each medium channel, while the other port was sealed using custom-made fluid stoppers. The two gel channel ports were initially punched in the PDMS with a 1 mm and 3 mm punch, respectively, and the 1 mm port (gel seeding port) was also sealed with a custom-made fluid stopper. Pressurization of the MVNs was achieved in the range 0 to 1000 Pa, in steps of 250 Pa. The Fluigent pressure regulator has the capability to deliver pressures up to 2500 Pa, but pressures above 1000 Pa resulted in interstitial flows that were too high to make reliable measurements. Permeability was measured as reported in [16]. Briefly, the perfused MVNs were imaged on a Olympus FV1000 confocal microscope with custom enclosure for temperature and atmosphere control, using a 10X objective at a resolution of 800x800 pixels. *Z*-stacks at least 100 μm deep were collected in steps of 5 μm at a time interval of 12 minutes. Image analysis was conducted using Fiji [45], and involved the automatic thresholding and segmentation of the fluorescent signal within the MVNs. Permeability, P, for a given fluorescent tracer was measured as [16]:

$$P = \frac{V_\mathrm{m}}{SA\,\Delta I}\frac{\Delta I_\mathrm{m}}{t} \tag{6}$$

Where V_m and SA are the matrix volume and MVN surface area, respectively, in the volume imaged, $\Delta I = I_{\mathrm{v},1} - I_{\mathrm{m},1}$ is the difference in fluorescence intensity between vasculature and matrix at the first time-point, and $\Delta I_\mathrm{m} = I_{\mathrm{m},2} - I_{\mathrm{m},1}$ is the increase in fluorescence intensity in the matrix

during a time interval *t*. In order to account for drift of the microscope and bleaching of the fluorescence, $I_{m,2}$ was normalized over the change in intensity within the MVN over time, assumed here constant, so that:

$$I^*_{m,2} = I_{m,2}\frac{I_{v,1}}{I_{v,2}} \quad (7)$$

For the fluid collection experiments, MVNs samples were perfused at 1000 Pa, and the extruded fluid from the device was manually collected every minute using a pipette placed above the gel in the large gel channel port.

Interstitial flow, hydraulic permeability and diffusion assessment: Interstitial flow velocity, *v*, as a function of position within the device was measured using a variation of the Fluorescence Recovery After Photobleaching (FRAP) technique, similar to what previously reported [46]. Samples were perfused with FITC-conjugated 70 kDa dextran overnight, during which time the tracer diffused uniformly within the gel matrix. Upon testing, the tracer was washed out of the MVN with fresh media, leaving darker traces (the MVNs) within a fluorescence-saturated matrix. The samples were then connected to the pressure regulator as described above and imaged on the confocal microscope, where the 488 laser was used to bleach a circular spot 30 μm in diameter over ≈ 2 s, followed by rapid image acquisition every 280 ms up to 10 s. Tracking of the bleached spot was performed using a MatLab plugin (frap_analysis), yielding the velocity of the bleached spot. The technique described assumes that the velocity of the bleached spot is that of the fluid flow, *i.e.* no impediment to the flow of solute through the hydrogel matrix, due its small size (a few nm [16]) compared to the microporosity of the material. It also assumes that flow occurs primarily in the *xy*-plane due to the homogeneity of the device in the *z* direction. The same technique was used in devices with only fibroblasts present in the matrix, cultured over seven days. Here, *v* was measured in the case of a pressure offset between the two side channels, Δp, which allowed the calculation of the hydraulic permeability of the matrix, *K*, as:

$$K = \frac{v}{(\Delta p/w)} \quad (8)$$

where w is the width of the gel channel, 3 mm. FRAP, in the absence of flow, was used to measure the diffusion coefficient of the various molecules assessed. The same methodology as above was used in matrix regions of devices with MVNs to bleach and record the recovery of the fluorescence within the spot. The frap_analysis MatLab plugin, in this case, yielded the diffusion coefficient, D_s, calculated based on the time required of the fluorescent tracers to self-diffuse within the bleached spot. This analysis assumes that the matrix is isotropic, so that 2D imaging of the bleached spot can be generalized to the 3D diffusion of tracer affecting recovery. The diffusion coefficient of the solutes in fluid was estimated using the Stoke-Einstein equation [47], assuming the medium viscosity as that of water [48], and taking the hydrodynamic radii for the dextrans and plasma proteins as those previously measured [16, 49].

Computational model of fluid flow in the MVNs: A 3D-1D numerical model was applied to describe the fluid flow within the central channel of the device between the two neck regions leading to the outlets. The model combines two different domains with different dimensionality: (i) a 3D domain, the gel region, and (ii) a 1D domain, the MVN. The methods used to perform the 1D reduction for the MVN are described in previous works [50-52]. The model describes the flow within the gel by means of Darcy's equation, and the flow in the MVNs with the Poiseuille equation for laminar, fully-developed flow, taking into account network junctions and filtration through the capillary membrane, which is described by Equation 1. The model was solved by means of the finite element method using the GetFem++ software, as previously shown [53,54]. The MVNs (1/4 of the length of the device, repeated spatially) were reconstructed from confocal images using the FIJI "skeletonize" function to compute the skeleton of the network. The viscosity of the media was set to 0.8 cP [55]. Boundary conditions were set to describe the experimental conditions: Fluid cannot exit the device through the top (PDMS) and the bottom (glass) surfaces. The same boundary condition was set at the surface

of the gel in contact with the neck leading to the closed gel port. At the monolayer on the lateral surfaces, the hydraulic conductivity was specified, spanning from 1X to 500X with respect to that of the MVNs.

Analysis of sampled interstitial fluid: Separate devices were used for each solute and repeat.1 µL of interstitial fluid collected at each time-point was diluted in 99 µL of phosphate buffered saline (PBS, VWR, US) and, in the case of fluorescently-labelled tracers (dextrans, plasma proteins, and Paclitaxel), analyzed using a Cytation 5 fluorescence plate reader (BioTek, US), at excitation/emission wavelengths of 490/530. Doxorubicin was also analyzed in the same plate reader, making use of its auto-fluorescence in the range 470-600. Proteins perfused through the system (plasma proteins, Trastuzumab, and Cetuximab) were analyzed through a sandwich ELISA, following further dilution 1:3 in PBS, and the absorbance signal was read on a SpectraMax M2 (Molecular Devices, US) at 450 nm with reference to 650 nm. An ELISA kit (ab108788, Abcam, US) was used for albumin as instructed by the manufacturer. Similarly, the monoclonal antibody pair HCA220-HCA228P (1 µg mL^{-1}) from BioRad, US, was used for Cetuximab. IgG and Trastuzumab were assessed using Amgen reagents, specifically mouse monoclonal antibodies recognizing human Fc (mu anti-hu Fc, 1.35.1 mAb, mu anti-hu Fc 21.1 mAb). For both fluorescence and ELISA analysis, assuming the detected signal varied linearly with concentration, a normalized concentration ratio was calculated for time-points within 5 and 10 minutes as:

$$\left(\frac{c}{c_0}\right)^* = \frac{c - c_B}{c_0 - c_B} \quad (9)$$

where c_B is the background concentration/signal obtained for medium perfused through the devices in the absence of any of the solutes tested.

Protein binding: Vasculife (1 mL) was spiked with each small molecule (Oregon Green paclitaxel or doxorubicin) to obtain a concentration of 5 µM. Triplicate 200 µL aliquots were transferred to 220 µL ultracentrifuge tubes and spun at 37°C and 225,000 x g for 2.5 hours in a

Beckman Coulter TLA-100 rotor. Twenty-five µL aliquots of spiked matrix were transferred to a sample plate and kept on ice to represent total drug. The remainder of spiked matrix was incubated at 37°C for the duration of the centrifugation period to be used as a stability control. After centrifugation, a 25 µL aliquot of the unbound fraction was transferred from each ultracentrifuge tube to the sample plate. 25 µL aliquots of the stability control matrix were also transferred to the sample plate. All samples were matched with an equal volume of blank matrix. Samples were extracted by adding three volumes of acetonitrile containing internal standard (1 µM tolbutamide) and 0.1% formic acid. Samples were vortexed, centrifuged at 4°C for 15 minutes at 3400 x g, and analyzed by LC-MS using a Thermo Q-Exactive in positive ion mode. Fraction unbound was calculated from the ratio of test article detected in the water layer after centrifugation relative to the total concentration in the original matrix.

Statistical analysis: Measurements of MVNs permeability were performed in three devices from three biological repeats. Flow collection results were obtained from four separate samples per solute, from three biological repeats, for which medium-only controls were always run. Data representation details are provided in the figure captions. Statistical significance was assessed using student's t-tests performed with the software OriginPro 2016, where differences at $p\text{-value} < 0.05$ were taken as significant. The same software was also used to perform linear fits of the data and analyze the significance and quality of fit of the trends observed.

Supporting Information

Supporting Information is available from the Wiley Online Library or from the author.

Acknowledgements

The authors thank Xuhai Be for help with the ELISA quantification. L.P. is thankful to the Fondazione Fratelli Agostino and Enrico Rocca under the Progetto Rocca doctoral fellowship. JLK is thankful to the European Research Council (ERC) under the Advanced Grant 'VESCEL' Program (Grant no. 669768).

Received: ((will be filled in by the editorial staff))
Revised: ((will be filled in by the editorial staff))
Published online: ((will be filled in by the editorial staff))

References

1. D. Huh, G. A. Hamilton, D. E. Ingber, *Trends Cell Biol.* **2011**, *21*, 754.
2. M.L. Schuler, *Lab Chip* **2019**, *19*, 9.
3. B. Godin, E. Touitou, *Adv. Drug Deliv. Rev.* **2007**, *59*, 1152.
4. Q. Gao, Z. Liu, Z. Lin, J. Qiu, Y. Liu, A. Liu, Y. Wang, M. Xiang, B. Chen, J. Fu, Y. He, ACS Biomater. *Sci. Eng.* **2017**, *3*, 399.
5. W.J. Polacheck, M.L. Kutys, J.B. Tefft, C.S. Chen, *Nat. Prot.* **2019**, *14*, 1425.
6. J. Nie, Q. Gao, Y. Wang, J. Zheng, H. Zhao, Y. Sun, J. Shen, H. Ramezani, Z. Fu, Z. Liu, M. Xiang, J. Fu, P. Zhao, W. Chen, Y. He, *Small* **2018**, *14*, 1802368.
7. M. Tabrizi, G.G. Bornstein, H. Suria, *AAPS J.* **2010**, *12*, 33.
8. L.I. Goulatis, E.V. Shusta, *Curr. Opin. Struct. Biol.* **2017**, *45*, 109.
9. M. Hammarlund-Udenaes, M. Friden, S. Syvanen, A. Gupta, *Pharm. Res.* **2008**, *25*, 1737.
10. T.S. Reese, M.J. Karnovsky, *J. Cell Biol.* **1967**, *37*, 207.
11. J. Scallan, V.H. Huxley, R.J. Korthuis, *Capillary fluid exchange*, Morgan & Claypool Life Science, San Rafael, CA, USA **2010**.
12. Z. Wang, C. Tiruppathi, R.D. Minshall, A.B. Malik, *ACS Nano* **2009**, *3*, 4110.
13. D.T. Wiley, P. Webster, A. Gale, M.E. Davis, *PNAS* **2013**, *110*, 8662.
14. M.B. Chen, J.A. Whisler, J.S. Jeon, R.D. Kamm, *Integr. Bio.* **2013**, *5*, 1262.
15. J.A. Whisler, M.B. Chen, R.D. Kamm, *Tissue Eng. Part C: Methods* **2014**, *20*, 543.
16. G.S. Offeddu, K. Haase, M.R. Gillrie, R. Li, O. Morozova, D. Hickman, C.G. Knutson, R.D. Kamm, *Biomaterials* **2019**, IN PRESS.
17. K. Haase, R.D. Kamm, *Regen. Med.* **2017**, *12*, 285.
18. W. Zhan, D.Y. Arifin, T.K. Lee, C.H. Wang, *Pharm. Res.* **2017**, *34*, 860.
19. S.Y. Yuan, R.R. Rigor, *Regulation of endothelial barrier function*, Morgan & Claypool Life Science, San Rafael, CA, USA **2010**.

20. J.R. Levick, C.C. Michel, *Cardiovasc. Res.* **2010**, *87*, 198.

21. P.M. Luckett, J. Fischbarg, J. Bhattacharya, S.C. Silverstein, *AM. J. Physiol.* **1989**, *256*, H1675.

22. R.L. Qiao, R. Sadurski, J. Bhattacharya, *Am. J. Physiol.* **1993**, *264*, L382.

23. J.A.M. Yaccino, Y.S. Chang, T. Hollis, T.W. Gardner, J.M. Tardbell, *Curr. Eye Res.* **1997**, *16*, 761.

24. Y.S. Chang, J.A. Yaccino, S. Lakshminarayan, J.A. Frangos, J.M. Tarbel, *Arteriosclerosis, Thrombosis Vasc. Biol.* **2000**, *20*, 35.

25. R.O. Dull, J. Yuan, Y.S. Chang, J. Tarbell, R.K. Jain, L.L. Munn, *Microvasc. Res.* **2001**, *61*, 203.

26. J.C. Parker, T. Stevens, J. Randall, D.S. Weber, J.A. King, *Am. J. Physiol.* **2006**, *291*, L30.

27. C.G. Hubert, S.W. McJames, I. Mecham, R.O. Dull, *Microvasc. Res.* **2006**, *71*, 135.

28. G. Li, M.J. Simon, L.M. Cancel, Z.D. Shi, X. Ji, J.M. Tarbell, B. Morrison III, B.M. Fu, *Annals Biomed. Eng.* **2010**, *38*, 2499.

29. E.S. Helton, S. Palladino, E.E. Ubogu, *Microvasc. Res.* **2017**, *109*, 1.

30. E.M. Renkin, *Circulation Res.* **1977**, *41*, 735.

31. H.K. Kimelber, Neuoscience **2004**, *129*, 851.

32. T.A. Nguyen, Y.A. Abdelhamid, L.K. Phillips, L.S. Chapple, M. Horowitz, K.L. Jones, A.M. Deane, *World J. Crit. Care Med.* **2017**, *6*, 28.

33. H. Maes, D. Olmeda, M.S. Soengas, P. Agostinis, *FEBS J.* **2016**, *283*, 25.

34. R.K. Reed, M.I. Townsley, A.E. Taylor, *Am. J. Physiol.* **1989**, 257, H1037.

35. C. Tiruppathi, W. Song, M. Bergenfeldt, P. Sass, A.B. Malik, *J. Biol. Chem.* **1997**, *272*, 25968.

36. H.L. Deissler, G.K. Lang, G.E. Lang, *Exp. Eye Res.* **2017**, *154*, 39.

37. J.E. Moore, C.D. Bertram, *Annual Rev. Fluid Mech.* **2018**, *50*, 459.

38. D.K. Shah, A.M. Betts, *mAbs* **2013**, *5*, 297.

39. L. Mohee, G.S. Offeddu, A. Husmann, M.L. Oyen, R.E. Cameron, *Acta Biomater.* **2019**, *83*, 189.

40. J. Baselga, *Eur. J. Cancer* **2001**, *37*, S16.

41. D. Gajria, S. Chandarlapaty, *Expert Rev. Anticancer Ther.* **2011**, *11*, 263.

42. I.F. Tannock, *BMC Cancer* **2010**, *10*, 255.

43. S. Curry, *Drug Metab. Pharmacokinet.* **2009**, *24*, 342.

44. M.B. Chen, J.A. Whisler, J. Frose, C. Yu, Y. Shin, R.D. Kamm, *Nat. Prot.* **2017**, *12*, 865.

45. J. Schindelin, I. Arganda-Carreras, E. Frise, V. Kaynig, M. Longair, T. Pietzsch, S. Preibisch, C. Rueden, S. Saalfeld, B. Schmid, J.Y. Tinevez, D.J. White, V. Hartenstein, K. Eliceiri, P. Tomancak, A. Cardona, *Nat. Methods* **2012**, *9*, 676.

46. N.J. Carroll, K.H. Jensen, S. Parsa, N.M. Holbrook, D.A. Weitz, *Langmuir* **2014**, *30*, 4868.

47. B. Amsden, *Macromol.* **1999**, *32*, 874.

48. E. Frohlic, G. Bonstingl, A. Hofler, C. Meindl, G. Leitinger, T.R. Pieber, E. Roblegg, *Toxicol. In Vitro* **2013**, *27*, 409.

49. J.K. Armstrong, R.B. Wenby, H.J. Meiselman, T.C. Fisher, *Biophys. J.* **2004**, *87*, 4259.

50. C. D'Angelo, A. Quarteroni, *Math. Models Methods Appl. Sci.* **2008**, *18*, 1481.

51. L. Cattaneo, P. Zunino, *Networks & Heterogeneous Media* **2014**, *9*, 135.

52. T. Koppl, E. Vidotto, B. Wohlmuth, P. Zunino, *Math. Models Method. Appl. Sci.* **2018**, *28*, 953.

53. L. Possenti, S. di Gregorio, F.M. Gerosa, G. Raimondi, G. Casagrande, M.L. Costantino, P. Zunino, *Int. J. Numer. Method. Biomed. Eng.* **2018**, e3165.

54. L. Possenti, G. Casagrande, S. di Gregorio, P. Zunino, M.L. Constantino, *Microvasc. Res.* **2018**, *122*, 101.

55. E.J. Lee, L.E. Niklason, *Tissue Eng. C* **2010**, 16.

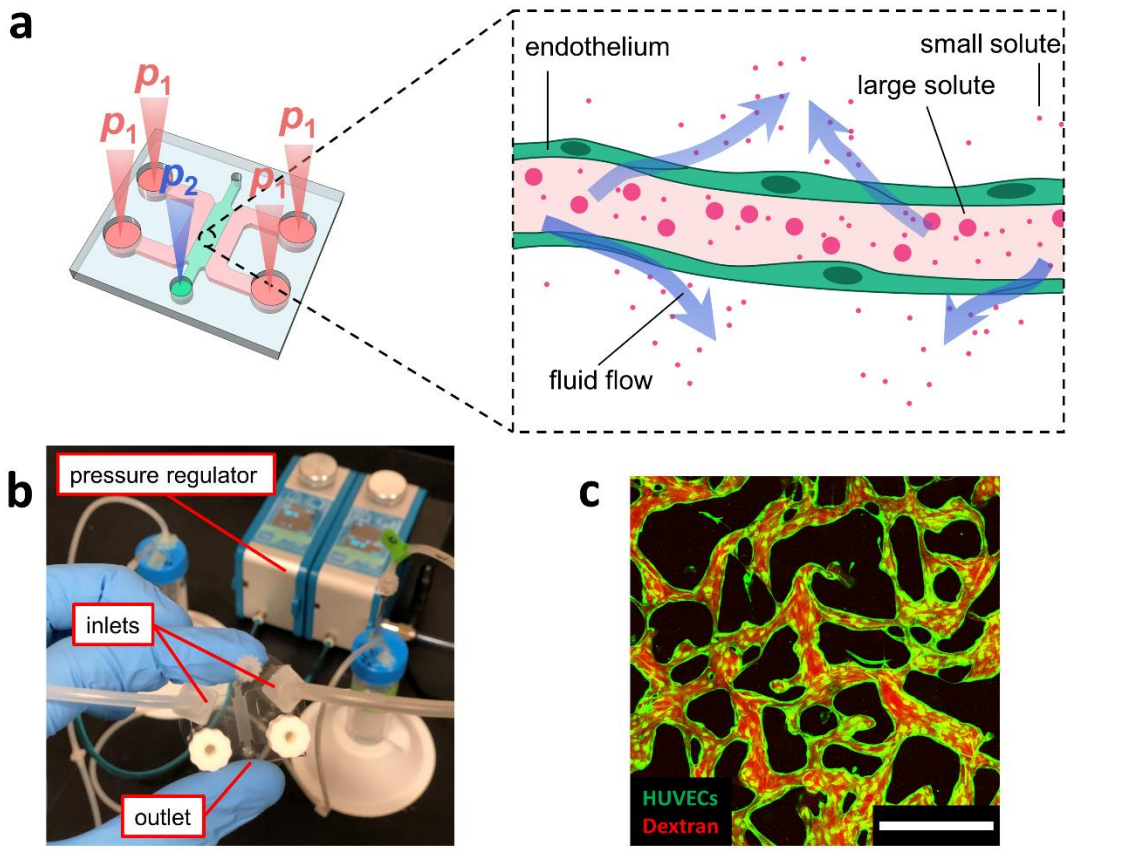

Figure 1. (a) Schematic diagram and (b) photograph of microfluidic device setup with applied pressure. Pressurization of the MVNs produces transmural flow and size-selective convective filtering of solutes across the endothelium that determines the trans-endothelial distribution of the solutes. In (a), p_1 represents the pressure applied in the media channels and p_2 the pressure at the gel outlet (atmospheric), where $\Delta p = p_1 - p_2 > 0$. A confocal microscopy image of the perfused MVNs is shown in (c); the scale bar is 200 μm.

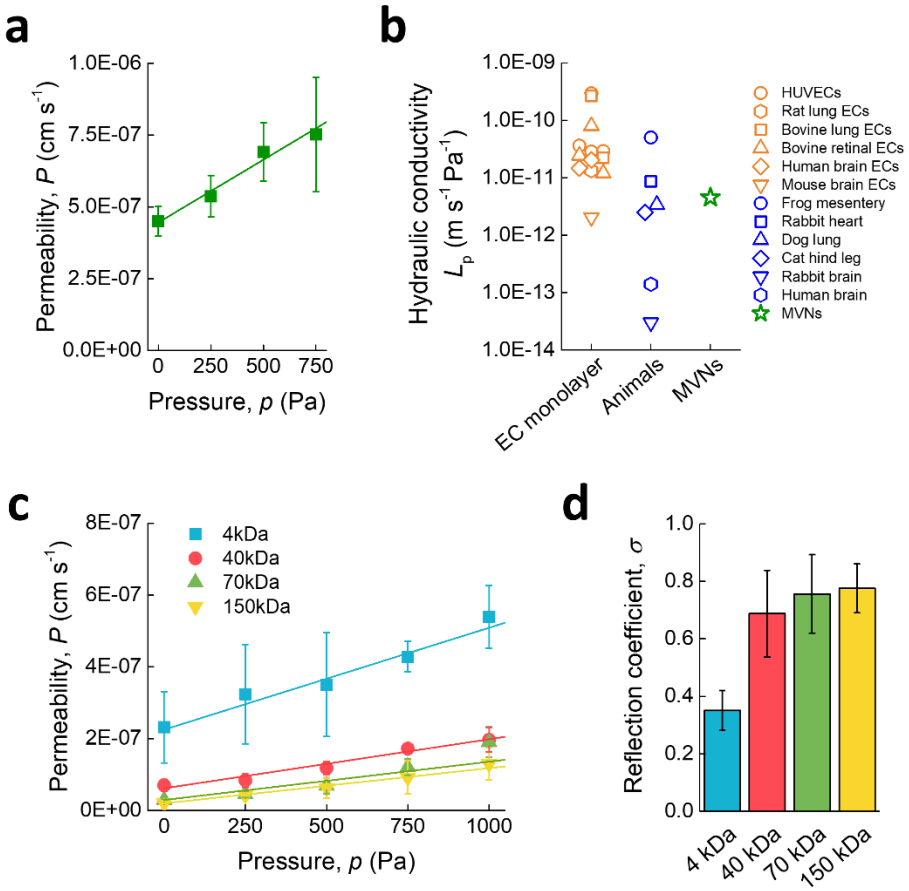

Figure 2. (a) Permeability (P) of the MVNs to FITC as a function of transmural pressure. The linear fit (solid line) was used to calculate the hydraulic conductivity (L_p) of the MVNs, compared in (b) to other *in vitro* systems and *in vivo* data. (c) Increase in P of the MVNs to dextrans of varying molecular weights with pressure. The linear fits (solid lines) yield the reflection coefficient (σ) for each solute, shown in (d). In (a), (c), and (d) data are reported as mean ± std. dev.

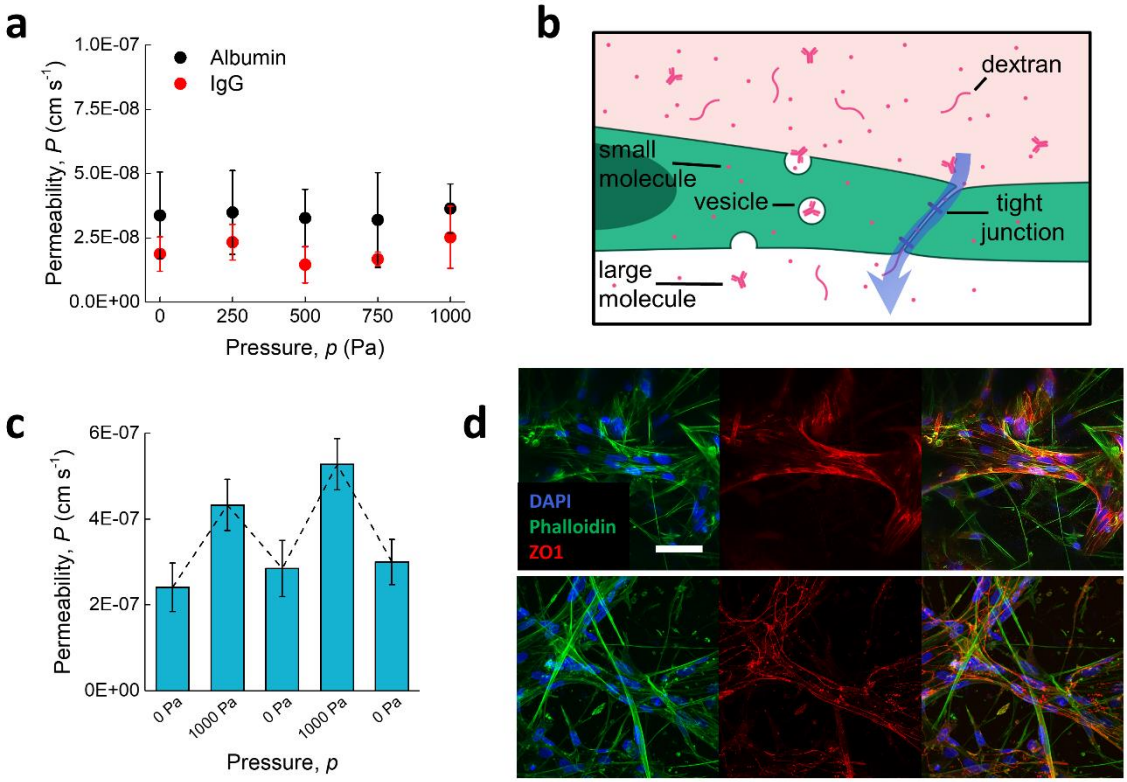

Figure 3. (a) Permeability (*P*) of the MVNs to plasma proteins (albumin and IgG) as a function of transmural pressure. (b) Schematic diagram of active vesicular transport and passive membrane diffusion (both flow-independent), and passive convection through junctions (flow-dependent) across the endothelium. Plasma protein binding of small molecules is not represented. (c) Hysteresis of *P* to 4 kDa dextran during a cycled pressure regime. (d) Confocal immunofluorescence staining of tight junctions between endothelial cells before (top) and after (bottom) flow. The scale bar is 50 μm. In (a), and (c), data are reported as mean ± std. dev.

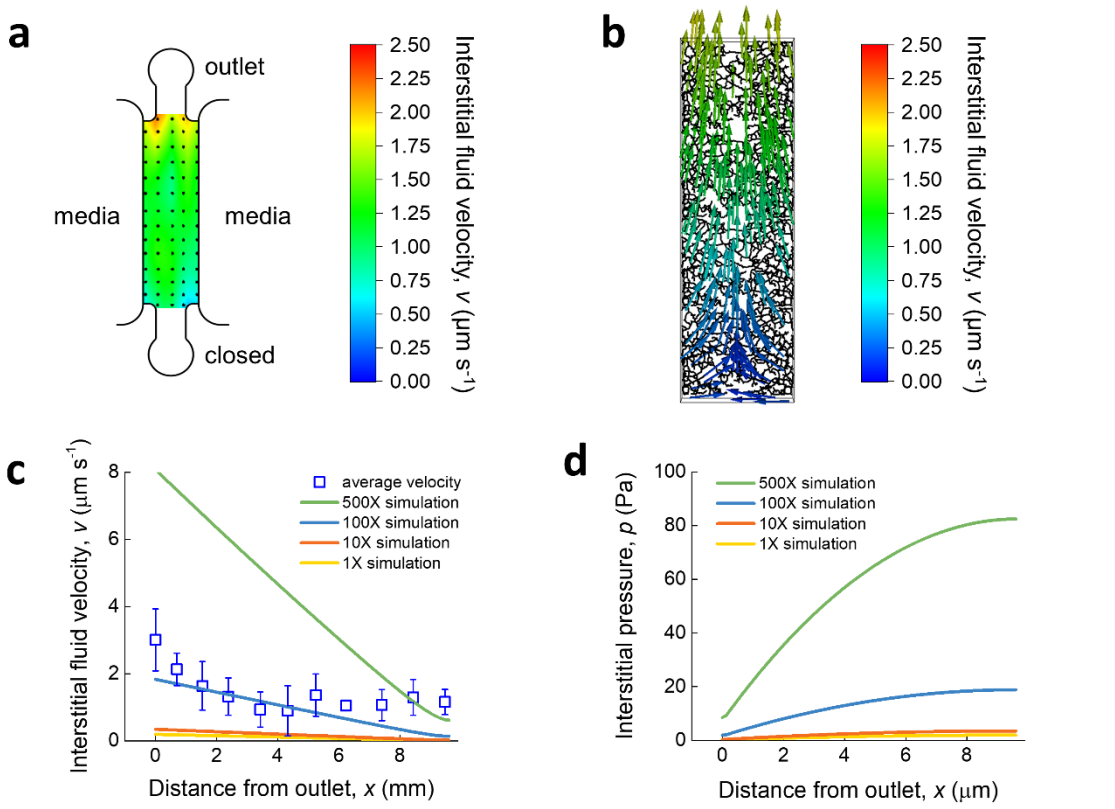

Figure 4. (a) Map of interstitial flow velocities (v) in the gel channel of the microfluidic device with pressure in the media channels set to 1000 Pa above the outlet pressure, and (b) corresponding computational simulation of flow velocity vectors. (c) Comparison of average interstitial flow velocity (mean ± std. dev.) as a function of distance from the device outlet with simulations for a range of monolayer hydraulic conductivities relative to that of the MVNs. In (d), the respective interstitial pressures (p) as a function of distance from the outlet are shown.

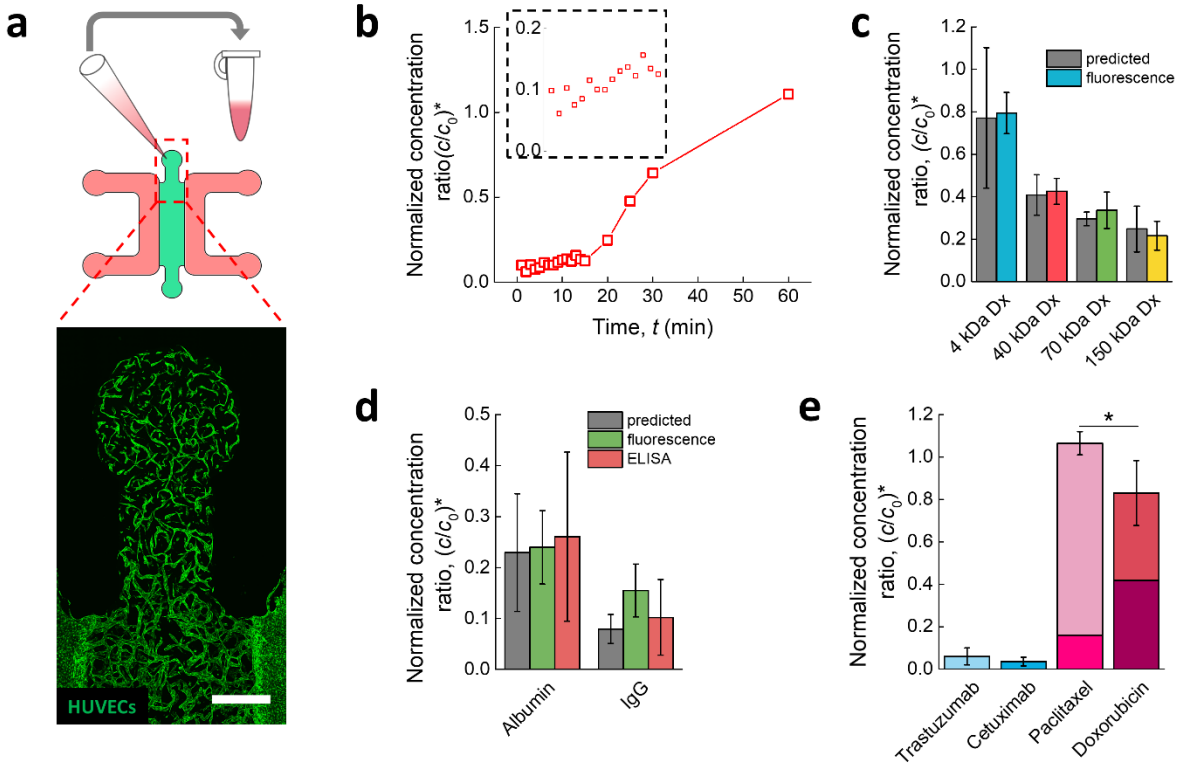

Figure 5. (a) Confocal microscopy image of MVNs near the outlet of the device, showing connected lumens extending up to the outlet, and schematic of the interstitial fluid collection process. The scale bar is 1 mm. (b) Relative concentration (c/c_0) of human FITC-labelled serum IgG sampled from the interstitial flow as a function of time, analyzed by fluorescence. The insert shows a scaled-up version of the data points up to 15 minutes. (c) Sampled c/c_0 of sampled dextran of varying molecular weight and (d) model proteins, compared to the predicted values using Equation 5. (e) Sampled c/c_0 of therapeutic molecules. For paclitaxel and doxorubicin, the overlaid bars represent the sampled concentrations (lower) and concentrations after adjustment for protein binding to plasma proteins (higher). Statistical significance assessed by student's t-test, * *p-value* < 0.05. In (c), (d), and (e) data are reported as mean ± std. dev.

Supporting Information

Direct sampling of therapeutics interstitial concentrations across perfused *in vitro* microvasculature

*Giovanni S. Offeddu, Luca Possenti, Joshua T. Loessberg-Zahl, Paolo Zunino, John Roberts, Sean Han, Dean Hickman, Charles G. Knutson, Roger D. Kamm**

Video S1. MVNs (HUVECs GFP) subjected to cyclic pressurization of 1000 Pa showing recoverable swelling.

Video S2. Bleaching of fluorescence within a spot of 30 μm diameter (far right of the field of view) at 0 Pa, *i.e.* in the absence of flow. Recovery of the fluorescence depends purely on self-diffusion of the fluorescent tracer. The field of view is 250 μm in lateral size.

Video S3. Bleaching of fluorescence within a 30 μm spot subjected to a 500 Pa flow right-to-left, and consequent translation of the spot across the field of view (250 μm in lateral size).

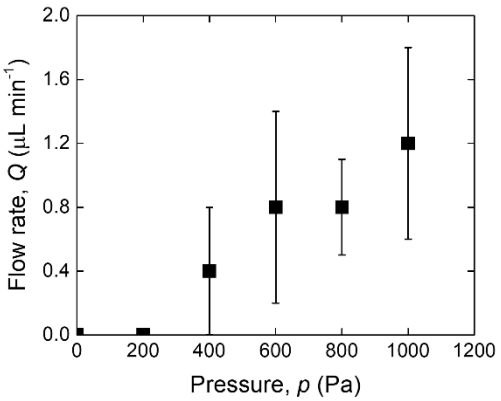

Figure S1. Flow rate (*Q*) of extruded fluid from the device outlet upon application of varying hydrostatic pressure in the medium. The data are expressed as mean ± std. deviation for two devices, for which the volume was estimated by collection with a pipette.

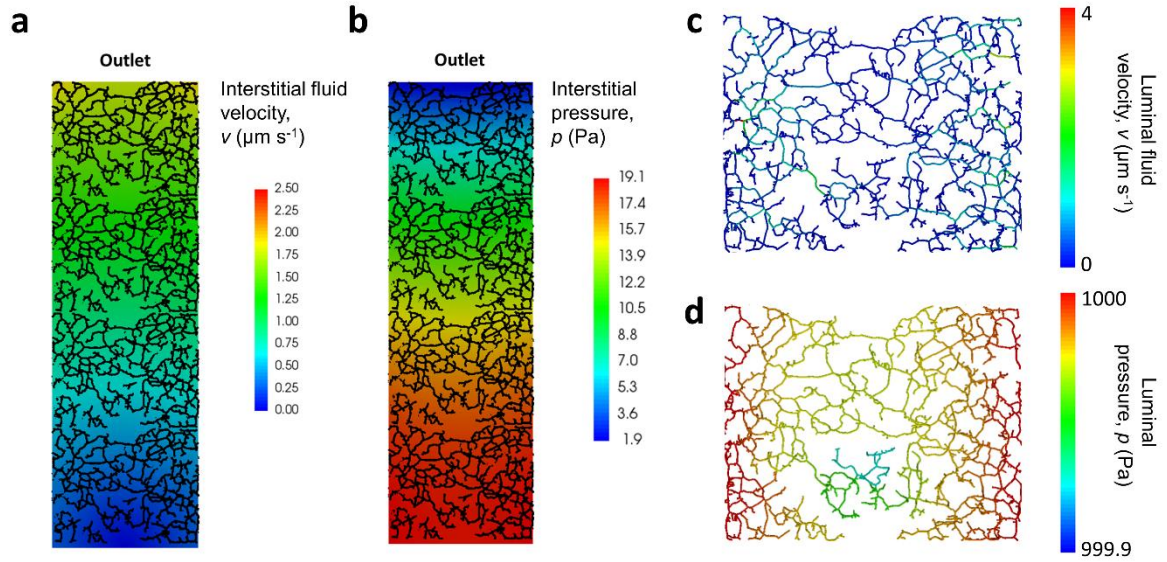

Figure S2. Computational simulation of (a) interstitial fluid velocity (*v*) and (b) interstitial pressure (*p*) as a function of position within the device, for an applied pressure of 1000 Pa. (c) Computational simulation of luminal *v* and (d) luminal *p* within the MVNs for the same condition.

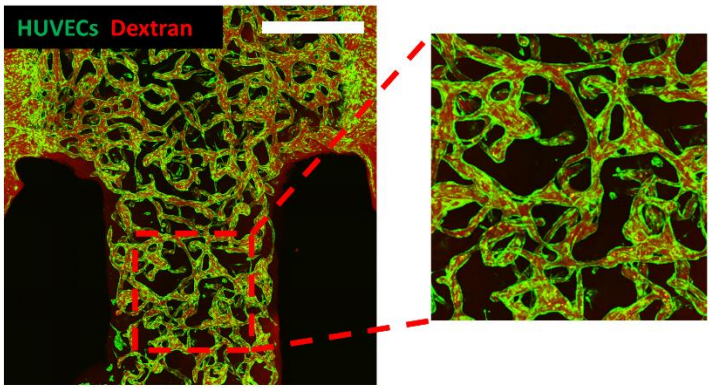

Figure S3. Mosaic confocal image of the device neck leading to the outlet. The MVNs can be here seen to be perfused with dextran (70 kDa), with an applied pressure of 1000 Pa. The scale bar is 1 mm.

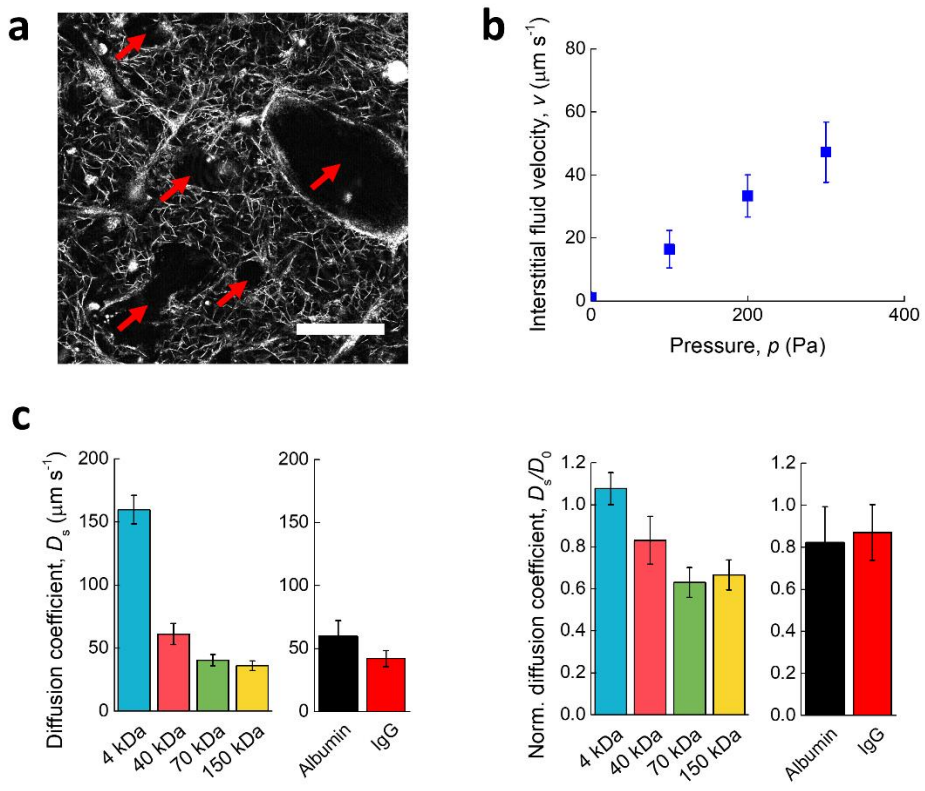

Figure S3. (a) Reflectance light image of the fibrin hydrogel matrix enclosing the MVNs, at day 7 of culture within the microfluidic device. The arrows indicate MVN lumens or possibly matrix remodelling; the scale bar is 50 μm. (b) Interstitial flow velocity (v) as a function of pressure drop between media channels. (c) Diffusion coefficient (D_S) of dextrans and model proteins within the gel matrix, and (d) corresponding coefficients normalized to the diffusion coefficient value in fluid (D_S/D_0). All data are reported as mean ± std. deviation.